energies

MDPI

Article

Smart Core and Surface Temperature Estimation Techniques for Health-Conscious Lithium-Ion Battery Management Systems: A Model-to-Model Comparison

Sumukh Surya [1,*], Akash Samanta [2], Vinicius Marcis [2] and Sheldon Williamson [2]

[1] Robert Bosch Engineering and Business Solutions, Bangalore 560100, India
[2] Department of Electrical, Computer and Software Engineering, Ontario Tech University, Oshawa, ON L1G 0C5, Canada; akash.samanta@ontariotechu.net (A.S.); vinicius.marcis@ontariotechu.net (V.M.); sheldon.williamson@uoit.ca (S.W.)
* Correspondence: sumukhsurya@gmail.com

Abstract: Estimation of core temperature is one of the crucial functionalities of the lithium-ion Battery Management System (BMS) towards providing effective thermal management, fault detection and operational safety. It is impractical to measure the core temperature of each cell using physical sensors, while at the same time implementing a complex core temperature estimation strategy in onboard low-cost BMS is also challenging due to high computational cost and the cost of implementation. Typically, a temperature estimation scheme consists of a heat generation model and a heat transfer model. Several researchers have already proposed ranges of thermal models with different levels of accuracy and complexity. Broadly, there are first-order and second-order heat resistor–capacitor-based thermal models of lithium-ion batteries (LIBs) for core and surface temperature estimation. This paper deals with a detailed comparative study between these two models using extensive laboratory test data and simulation study. The aim was to determine whether it is worth investing towards developing a second-order thermal model instead of a first-order model with respect to prediction accuracy considering the modeling complexity and experiments required. Both the thermal models along with the parameter estimation scheme were modeled and simulated in a MATLAB/Simulink environment. Models were validated using laboratory test data of a cylindrical 18,650 LIB cell. Further, a Kalman filter with appropriate process and measurement noise levels was used to estimate the core temperature in terms of measured surface and ambient temperatures. Results from the first-order model and second-order models were analyzed for comparison purposes.

Keywords: electric vehicles; stationary battery energy storage system; battery automated system; online state estimation; thermal modeling; first-order model; second-order model; Kalman filtering

check for updates

Citation: Surya, S.; Samanta, A.; Marcis, V.; Williamson, S. Smart Core and Surface Temperature Estimation Techniques for Health-Conscious Lithium-Ion Battery Management Systems: A Model-to-Model Comparison. *Energies* **2022**, *15*, 623. https://doi.org/10.3390/en15020623

Academic Editor: Haifeng Dai

Received: 14 November 2021
Accepted: 4 January 2022
Published: 17 January 2022

Publisher's Note: MDPI stays neutral with regard to jurisdictional claims in published maps and institutional affiliations.

Copyright: © 2022 by the authors. Licensee MDPI, Basel, Switzerland. This article is an open access article distributed under the terms and conditions of the Creative Commons Attribution (CC BY) license (https://creativecommons.org/licenses/by/4.0/).

1. Introduction

Lithium-ion batteries (LIBs) have been extensively commercialized as a primary energy storage technology for electric vehicles (EVs), stationary energy storage in the smart grid system and several other consumer electronics. The primary dominating factors of LIBs over other energy storage technologies include high energy density, long lifespan, and declining cost [1–4]. However, from literature and practice, it is noticed that the performance of LIBs as well as the durability and reliability are significantly influenced by the operating temperature. Moreover, excessively high temperatures may cause thermal runaway, leading to fire, smoke and other serious safety hazards to the operators [5–7]. Therefore, the requirement of a battery management system (BMS) has become indispensable for effective thermal management and safety of LIB system, which essentially requires accurate information on the core and surface temperature of each cell [8,9] besides other important states such as state of charge (SOC) [10,11] and state of health (SOH). A few other popular functions of an advanced BMS include cell balancing [12,13], fault detection/diagnosis [14]

and some other safety inspection functionalities. Several recent research studies highlighted that the accuracy of estimating cell SOC [15], SOH [16] and remaining storage capacity [17] depends on the accurate estimation of cell temperature as all these states are the function of temperature. Moreover, the Columbic efficiency of a cell is greatly affected by the cell temperature during the charging and discharging period. It is worthwhile to mention that the temperature distribution inside the cell is not uniform, and the core temperature remains higher than the surface temperature during practical application, especially under high charging and discharging current [18]. Typically, the difference between the core and surface temperature varies in the range of 5–10 °C [19,20]; however, under high current loading with rapid load fluctuation, it could be even more. Therefore, accurate information on the core and surface temperature is essential to achieving the effective thermal management of an LIB pack besides fault detection. While most of the existing temperature measurement techniques measure the surface temperature directly using physical sensors [21], the measurement of cells' internal temperature is highly challenging when using a physical sensor. Moreover, any high-capacity LIB pack consists of thousands of single LIB cells; thus, installing physical sensors in each cell is not practically feasible from the viewpoint of incremental cost and manufacturing complexity.

To sum up, accurate information on core temperature undoubtedly serves as the essential basis for the thermal management and safety of LIB apart from SOC and SOH estimation whilst it is difficult to measure the core temperature using physical sensors. Therefore, a precise thermal model is crucial to accurate temperature estimation. Moreover, it should be easy to model and computationally inexpensive in order to be implemented in onboard BMS for online prediction of temperature. Several temperature estimation techniques have been proposed by researchers. Typically, a temperature estimation strategy consists of two models, namely, a heat generation model and a heat transfer model [22]. The heat generation model takes physical measurement signals from a cell, typically voltage current, to estimate the total heat generation during charging and discharging. Then, the heat transfer model takes the estimated total heat quantity as model input to predict the temperature of that cell. Depending on the modeling, it can only estimate the core temperature (single-state) or both the core and surface temperature simultaneously (two-state).

Broadly, heat generation models can be classified into three groups, electrochemical models [23–26], data-driven empirical models [27–29] and equivalent circuit models (ECM) [30–32]. Few other researchers have also grouped the heat generation model from the perspective of heat concentration. According to them, the heat generation model could be a concentrated model (all heat is generated at the core), distributed model (heat generated uniformly over the cell) [33] and heterogeneous model [30,34] (due to temperature and current density gradient inside the cell). On the other hand, the heat transfer model can be grouped into finite element analysis (FEA)-based models [32,35–38], lumped multi-node models [27,39–41] and heat capacitive-resistive models [42]. The lumped multi-node model and heat capacitive-resistive models are typically developed based on the analogy between thermal and electrical phenomena. It can be seen that the electrochemical model can produce a very accurate heat generation value provided all model parameters are carefully tuned. However, the electrochemical models are highly complex and computationally expensive. The accuracy of data-driven empirical models highly depends on the experimentally acquired data. Collecting such high-resolution data is challenging, and with the increase in data volume and the number of feature vectors, computational expenses also increase exponentially. On the other hand, an ECM-based estimation model can be designed suitable for online prediction and real-world application by establishing a balance between the computational cost and prediction accuracy. Therefore, ECM-based battery models are extensively used in practice for estimating heat generation in LIB. Further, as far as the heat transfer model is concerned, the heat resistor–capacitor models are easy to develop and computationally efficient compared to FEA-based methods and lumped-parameter multi-node models. The FEA-based methods are highly accurate; however, they come at

the expense of a high computational cost. Resistor–capacitor-based models can be optimally engineered to make a balance between prediction accuracy and computational cost depending on the application requirement. Therefore, heat resistor–capacitor model-based temperature estimation is the prime focus of this present study.

Researchers have proposed different kinds of heat resistor–capacitor models for the accurate and precise internal and surface temperature estimation of LIB. However, the major concern regarding the practical application of any model is its computational cost, the capability of online prediction and suitability for onboard BMS. Detailed studies on the thermal characteristics of different layers inside an LIB cell, modelling complexity and the experimental data requirement have been carried out and are listed in the references section [43–48]. The heat resistor–capacitor models use the analogy between thermal and electrical phenomena, where heat capacity (thermal capacitance) and heat transfer coefficient (thermal resistance) are represented as electrical capacitor and resistor, respectively [43]. So far, a first-order (one thermal energy storage element) and second-order (two thermal energy storage elements)-based thermal models have been reported in the literature for temperature estimation. Second-order models are typically complex and require extensive experiments alongside the knowledge of domain experts during modeling. On the other hand, first-order models are easy to implement, computationally inexpensive and require far fewer experiments. Recently, extensive research effort has been made on second-order thermal models of LIB. However, a comparative study between the first-order and second-order model has not yet been assessed. Therefore, this research study focused on the comparative study to investigate whether it is worth investing in developing and implementing a second-order thermal model for the core temperature estimation of LIB in terms of accuracy, modeling complexity and the experimental requirement and its practicability in onboard BMS. Extensive experiments were conducted for data collection, and the data was further utilized for modeling, validation and comparison purposes. The strategy was to employ an ECM-based heat generation model for both a first-order and second-order thermal model to determine the total heat generation inside the cell. A Kalman filter (KF) was used in both the cases to improve prediction performance. Then, the estimation results were compared with the measured data to assess the modeling accuracy. Finally, the predicted results obtained from the first-order and second-order model were compared for the purpose of model-to-model comparison.

The remaining portion of the article is subdivided into five sections for better readability, representation and understanding of the readers. First-order and second-order thermal modeling of LIB and the respective temperature estimation strategy are presented in Section 2. The experimental setup and model parameter identification are discussed in Section 3. Temperature estimation using the fusion of the first-order thermal model with KF and second-order thermal model with KF is described in Section 4. Section 4 also includes the comparative study between the first-order thermal model and second-order thermal model in terms of prediction accuracy and modeling complexity. Major findings and concluding remarks are drawn in the conclusion in Section 5.

2. Thermal Modeling and Temperature Estimation Strategy

Commercially, LIBs are available in many different form factors such as prismatic cells, pouch cells [49] and cylindrical cells. Among these, cylindrical cells are widely used in large-scale high-power applications. However, the cylindrical cell has worse thermal heat dissipation, and the spiral format leads to a big thermal gradient inside the cell. Therefore, the thermal modeling of a 18,650 cylindrical LIB cell is considered in this study, considering the necessity of effective thermal management of cylindrical LIB. The mathematical analysis and the fusion of KF with these thermal models for core and surface temperature estimation are presented in this section. The aim is to provide a guideline for selecting an appropriate thermal model for online prediction with an optimum computational cost suitable for onboard low-cost BMS. As previously discussed in the introduction section, the temperature estimation model consists of one heat generation

model and a heat transfer model, where the heat generation model provides input to the heat transfer model. Therefore, the modeling strategy and mathematical analysis of the ECM-based heat generation model are considered here as well.

2.1. Heat Generation Model

The Electric Circuit Model (ECM) [50]—based thermal estimation model has been reported to estimate the total heat generation inside the LIB cell by several researchers. So far, electrochemical modeling has demonstrated the best performance in capturing the nonlinearities of LIB, while at the same time, it is the most complex to model. Capturing the high degree of nonlinearities higher-order ECM is required; however, the computational cost and modeling complexity increase with the increase in model order. Yet the major advantage of ECM is that a balance between the modeling complexity and model accuracy can be achieved through optimization with the help of the model order reduction technique [51,52]. Therefore, a 1-RC (first-order) ECM is considered here to quantify the total heat generation. The 1-RC ECM of LIB is shown in Figure 1. The basic strategy used by any ECM-based heat generation model is to mathematically accumulate the heat generation from internal power losses that typically depend on the internal resistance and charging–discharging current level. Again, the heat generation depends on the cell SOC, current level and temperature, as the internal resistances are the functions of these variables.

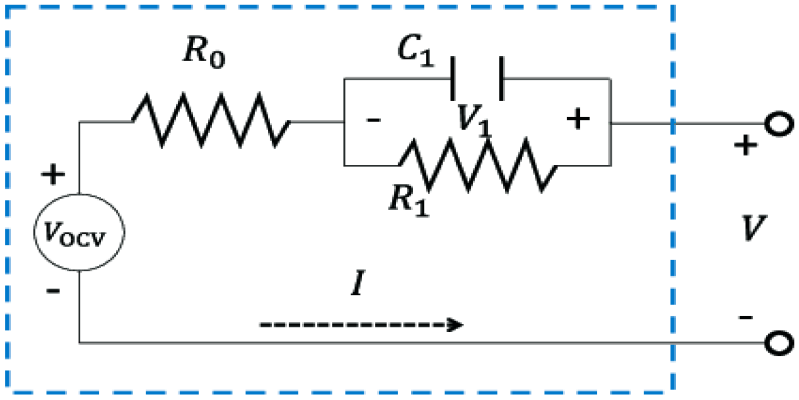

Figure 1. 1-RC ECM (Thevenin's equivalent) model of an LIB cell.

The V_{OCV} and V in Figure 1 represent the open-circuit voltage and the terminal voltage, respectively. The steady-state DC series resistance, which represents the electrolyte resistance to the lithium-ion transportation, is denoted as R_0 in Figure 1. Further, the short transient response is caused by the lithium-ion flow in the solid electrolyte interphase layer, and the anode electrode is represented by polarization resistance (R_1) and capacitance (C_1), respectively. These R_1 and C_1 appear only during the transient period [53]. A 1-RC battery model was considered in this study due to its optimum performance, ease of modelling, low computational cost and adequate accuracy when compared to other higher-order RC models [54,55]. Further, the online determination of heat generation inside LIB with these higher-order models is challenging due to computational cost. For this, Bernardi et al. [56] developed a simplified equation for LIB heat generation calculationthatis suitable for online prediction over other computationally expensive methods such as constant heat generation rate [57], curve fitting technique [58] and Joule's Law [59]-based methods. The governing equation for the total heat generated inside the battery (Q) as developed by Bernardi et al. [56] is shown in Equation (1).

$$Q = I(V - V_{OCV}) \tag{1}$$

The parameters of this equation are also the function of charging–discharging current (I), SOC and temperature, which are estimated using the ECM of the cell. Finally, the

value of the Q, obtained from Equation (1), is used as one of the inputs to the first-order and second-order thermal model for temperature estimation, which is discussed in the following section.

2.2. First-Order Thermal Modelling

2.2.1. Mathematical Analysis of First-Order Thermal Model

Now, for the first-order model, as is noted by several other researchers, the surface temperature is considered constant throughout the surface of the cell. Heat transport is only along the radial direction, meaning the lateral surface temperature is considered the same as axial direction (cell temperature at two terminals), as reported in [43]. Further, regarding heat transfer, only heat conduction from the core to the surface is considered. Heat exchange between surface and ambient by convection is not considered. The first-order thermal model is depicted in Figure 2.

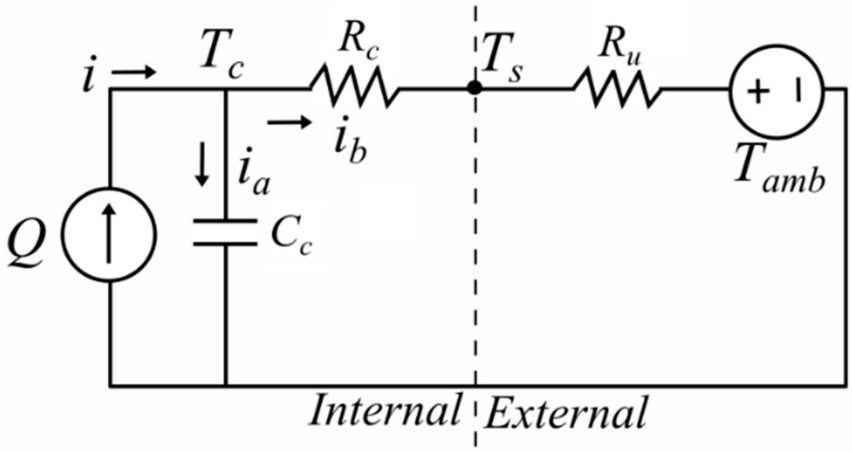

Figure 2. First-order heat resistor–capacitor-based thermal model of LIB.

In Figure 2, the thermal parameters, that is, the heat capacity of the core, heat transfer resistance inside the cell, heat transfer resistance outside the cell and total quantity of heat liberated concentrated from the core, are represented by C_c (J/K), R_c (K/W), R_u (K/W) and Q (J), respectively. The unit of each respective quantity is mentioned in the parentheses. The temperature of the core, surface and ambient is represented by T_c, T_s and T_{amb}, respectively, measured in K. The core temperature at node T_c and surface temperature at node T_s can be monitored using this model; thus this type of model is also referred to as a two-node or two-state thermal model [22,60].The heat resistor–capacitor model uses the analogy between the thermal and electrical systems, as discussed in the introduction section. Thus, for mathematical analysis, the heat transfer rate is represented by electrical current (i), and the branch currents are represented by i_a, i_b in the respective branch, as shown in Figure 2. Therefore, the governing equation of the model can be derived by applying Kirchhoff's Current Law (KCL) at the T_c node. The current balance equation at node T_c reads:

$$i = i_a + i_b = Q \tag{2}$$

Now, by rewriting Equation (2) in terms of thermal parameters, Equation (3) can be found:

$$Q = C_c \frac{dT_c}{dt} + \frac{T_s - T_c}{R_u} + \frac{T_{amb} - T_s}{R_c} \tag{3}$$

By re-arranging Equation (3) we find:

$$C_c \frac{dT_c}{dt} = Q + \frac{T_s - T_c}{R_u} + \frac{T_{amb} - T_s}{R_c} \tag{4}$$

Finally, the value of T_c can be calculated by integrating Equation (4) with respect to the total heat transfer time while the values of T_s and T_{amb} are known. While T_{amb} can be easily measured by employing only one temperature sensor, the measurement of T_s with physical sensors in a high-power LIB pack is challenging. Therefore, the alternative solution is to estimate the surface temperature using a temperature estimation scheme. One such estimation scheme is also proposed in reference [8], which estimates T_s from known T_c.

2.2.2. KF for First-Order Thermal Model

KF is used to estimate and predict an unknown parameter from known parameters. The state model for a KF and the first-order model, as developed in the reference [43,61] and in [62] respectively, are also considered for this study. Now, assuming the state as $T_{c,t}$, output as $T_{s,t}$ and inputs as Q and T_{amb}, The state-space matrices are derived by linearizing Equation (4) in the discrete domain. A linearized version of Equation (4) is shown in Equation (5).

$$T_{c,t} - T_{c,t-1} = \frac{Q_{t-1}}{Cc} + \frac{T_{s,t-1} - T_{c,t-1}}{C_c R_c} + \frac{T_{amb,t} - T_{s,t-1}}{C_c R_u} \tag{5}$$

As shown in reference [8], small changes in T_s can be ignored. Hence, the term $T_{s,t-1}$ can be considered as zero.

$$T_{c,t} = \frac{Q_{t-1}}{Cc} + T_{c,t-1}(1 - \frac{1}{C_c R_c}) + \frac{T_{amb,t-1}}{R_u C_c} \tag{6}$$

The transfer matrices of the KF-based temperature estimation model can be found by reducing Equation (6) in the form of state models as shown in Equations (7)–(9).

Hence,

$$\mathrm{A} = [1 - \frac{1}{C_c R_c}] \tag{7}$$

$$\mathrm{B} = [\frac{1}{C_c} \quad \frac{1}{C_c R_u}] \tag{8}$$

$$\mathrm{C} = D = 0 \tag{9}$$

2.3. Second-Order Thermal Modelling

2.3.1. Mathematical Analysis of Second-Order Thermal Model

The condition of non-uniform T_s and heat transport in the radial direction through conduction from the core to surface is also considered during the second-order thermal modeling. Additionally, the heat exchange between the surface and ambient is considered in the second-order model, which was not included in the first-order model. Only convective heat exchange between the cell surface and ambient is considered here. Therefore, in addition to the thermal properties of the first-order model, the thermal capacitance of cell case (C_s) is also considered. The resulting equivalent circuit of the second-order thermal model using heat resistor–capacitor is shown in Figure 3, similarly to the findings of other studies [8,60,63,64].

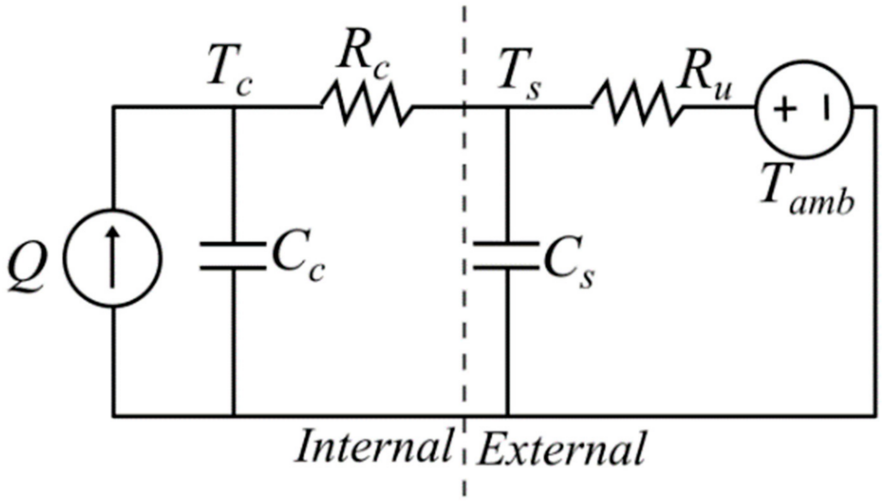

Figure 3. Second-order equivalent circuit thermal model of LIB.

Q needs to be estimated for the same ECM-based strategy mentioned in Section 2.1. To derive the mathematical analysis of the second-order thermal model, heat balance analysis in the core and surface is performed. The heat balance equation at the core and surface is represented in Equations (10) and Equation (11), respectively [8].

$$C_c \frac{dT_c}{dt} = Q + \frac{T_s - T_c}{R_c} \tag{10}$$

$$C_s \frac{dT_s}{dt} = \frac{(T_{amb} - T_s)}{R_u} - \frac{(T_s - T_c)}{R_c} \tag{11}$$

2.3.2. KF for Second-Order Thermal Model

T_c could be estimated by re-arranging the coupled ordinary differential equations of the second-order thermal model. Since the thermal model has two thermal energy storage parameters (C_c and C_s), two governing equations are used to estimate T_c in terms of measured T_s and T_{amb}.

$$\mathbf{A} = [1 - \frac{1}{C_c(R_c + R_u)}] \tag{12}$$

$$\mathbf{B} = [\frac{1}{C_c} \quad \frac{1}{C_c(R_c + R_u)}] \tag{13}$$

$$\mathbf{C} = [\frac{R_u}{R_c + R_u}] \tag{14}$$

$$\mathbf{D} = [0 \quad \frac{R_c}{R_c + R_u}] \tag{15}$$

It is worth noting that C_c, R_c and R_u in the second-order thermal model are the same as C_p, R_{in} and R_{out}, respectively, in the first-order model.

2.3.3. Fundamentals of KF

It is worth providing a basic explanation of KF as it is the heart of the temperature estimation scheme discussed here. A KF is a linear quadratic estimator and is mainly used in statistics and control engineering. It outputs the estimates of an unknown state and uses the noise and the inaccuracies of the measured output. Some of the common examples of KF usage include guidance, navigation and core temperature estimation in EVs; the general form of KF is shown below:

$$X_k = A_{k-1}X_{k-1} + B_{k-1}U_{k-1} + W_{k-1} \tag{16}$$

$$Y_k = C_k X_k + D_k U_k + V_k \tag{17}$$

where X_k is the state of the system ($T_{c,t}$), Y_k is the output of the system ($T_{s,t}$), U_k is the input to the system ($[T_{amb,t}\ Q]^T$), t presents the state of the system and $t-1$ represents the previous state of the system. The block diagram of a KF is shown in Figure 4. It is a robust and simple technique used to estimate data based on its input signal. It uses mathematical modeling of the system and by giving the same input as an actual system, it predicts the output. The measured output from the actual system and predicted output from the mathematical model are then compared to obtain the error. This error is multiplied with Kalman gain and is added to the predicted state to obtain an accurate estimated state [65].

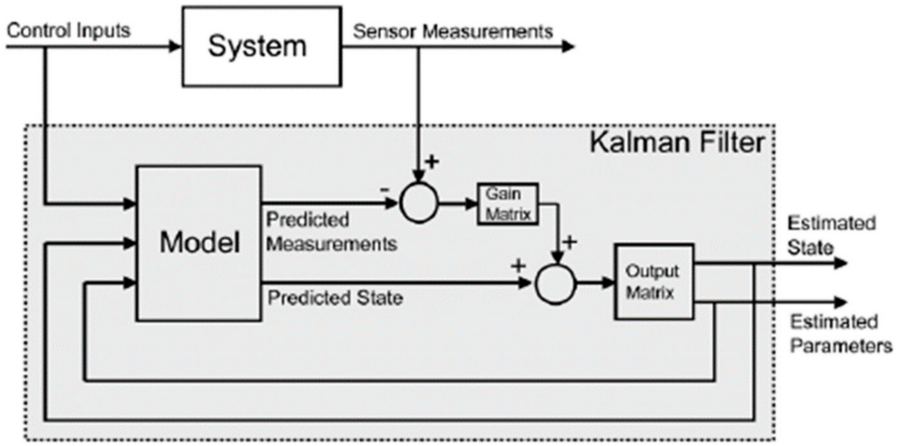

Figure 4. Fundamental building blocks of KF based estimation scheme.

3. Experimental Analysis for Thermal Model Parameterization

An automated battery testing system is the best option to collect battery test data, especially for an LIB, as LIB cells are highly sensitive to voltage, current, temperature and other environmental uncertainties. Therefore, an in-house "Battery Automated System (BAS)" was previously developed by the research group of Smart Transportation Electrification and Energy Research (STEER). The setup was used to invent the constant temperature constant current (CT-CV) charging technique [66,67] and several other prominent research studies in the BMS domain [2,4,8]. The BAS is an experimental setup with a fully programmable test environment control and data acquisition system. A schematic layout of the BAS is shown in Figure 5. The experimental data were then used for the parameter estimation of ECM and thermal modeling, model validation and model-to-model comparison purposes. Interested readers are invited to refer to these papers [2,4,8,66,67] for more details about the experimental setup. However, a brief overview of the experimental setup and test conditions is also mentioned in this section as a quick reference for the readers. The basic idea was to identify the input parameters of the thermal model, that is, heat capacity and heat transfer coefficients, through a steady-state analysis as well as transient experiments based on the nonlinear least square algorithm. The LIB cell was tested at three different temperatures where the internal battery temperature was raised using standard current pulses that were within the permissible limit specified on the manufacturer datasheet to ensure no capacity fade occurred during testing.

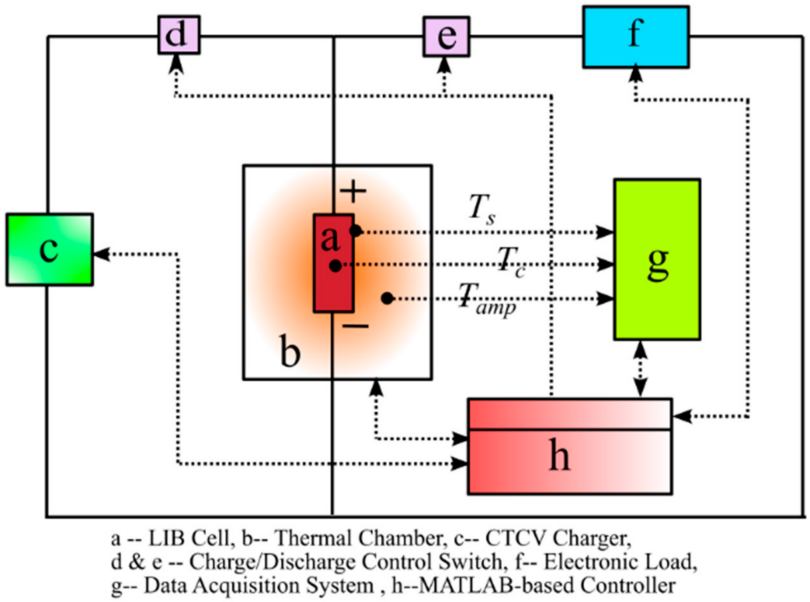

Figure 5. Schematic layout of the Battery Automated System (BAS).

Experimental Setup

Battery testing was performed on a 18,650 NMC (Lithium Nickel Manganese Cobalt Oxide) LIB, manufactured by LG Chem. Detailed specifications of the cell as provided by the manufacturer are mentioned in Table 1. A programmable power supply (Model: E36313A) from Keysight and a programmable electronic load (Model: BK8601) from B&K Precision were used for charging and discharging the battery with a predefined charging–discharging current profile. Further, a programmable temperature chamber was used to maintain the T_{amb} based on a predefined set-point. Finally, to control the BAS a MATLAB script-based program was used. A programmable data acquisition system (DAQ) (model DPM66204) from Chroma was used to collect the cell voltage, current and temperature data. Different current profile sat three different ambient temperatures (T_{amb} = 273 K (0 °C), 293 K (20 °C) and 323 K (50 °C)) were used for charging and discharging experiments. Finally, a nonlinear least square algorithm was used for online parameter estimation for developing the ECM and thermal model as demonstrated by Surya et al. [8]. All the model components were designed in MATLAB using three-dimension interpolated look up tables where the feature vectors were SOC, I_{bat} and T_{amb}. The heat generation model and the first-order and second-order thermal model were also developed in the MATLAB/Simulink and Simscape environment. Finally, an extensive simulation study was conducted to collect the simulated core and surface temperature data for further analysis. Simulation results were used for model validation as well as model-to-model comparison between the first-order and second-order thermal models. The core temperature (T_c) was estimated using a KF for various patterns of currents that were within the permissible limit specified on the manufacturer datasheet to ensure no capacity fade occurred during testing.

Table 1. Specifications of 18,650 LIB cell under test.

Specification Name	Values
Manufacturer and Model	LG Chem/INR18,650HG2
Cell Form Factor	Cylindrical (18,650)
Chemistry	Lithium Nickel Manganese Cobalt Oxide ($LiNiMnCoO_2$)
Nominal Voltage	3.6 V
Nominal Capacity	3 Ah
Standard Charging (CC-CV)	1.5 A, 4.2 V, Cut-off: 50 mA
Fast Charging (CC-CV)	4.0 A, 4.2 V, Cut-off: 100 mA
Discharging Condition	20 A (Max. Current), 2.5 V (Cut-off Voltage)
Operating Temperature	Charge: 0 to 50 °C, Discharge: −30 to 60 °C
Pack Weight	48 g

4. Results and Discussion

This research study intended to answer whether it is worth developing a second-order model instead of a first-order model for online temperature prediction by low-cost onboard BMS, firstly, by developing a first-order and second-order thermal model utilizing battery test data and MATLAB-based online parameter estimation; secondly, by simulating the temperature profile of the cell using the first-order and second-order thermal models subjected to different current profiles. The intention was to investigate the impact of charging–discharging current on the core and surface temperature of the cell. Thirdly, we compared the estimation results obtained from the first-order and second-order models. All simulations were carried out in the MATLAB Simulink environment, where a fixed solver and an appropriate step time were used [62]. Initially, simulation was carried out without employing a KF to deduce the baseline analysis. Figure 6 shows the current profile used for the base case analysis, and Figure 7 shows the plots of estimated T_c, T_s and the measure T_{amb}. Previously, we measured T_s from experiments. By comparing the measured and estimated T_s it was observed that both T_s were within the acceptable limit, and T_c and T_s closely followed the current profile, and $T_c > T_s > T_{amb}$, as per the expectation, confirming the modeling accuracy.

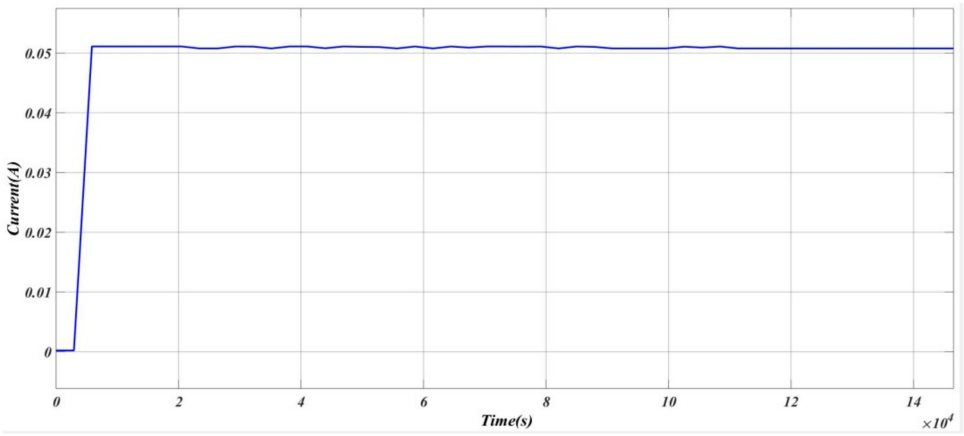

Figure 6. The pattern of the discharging current applied to the cell.

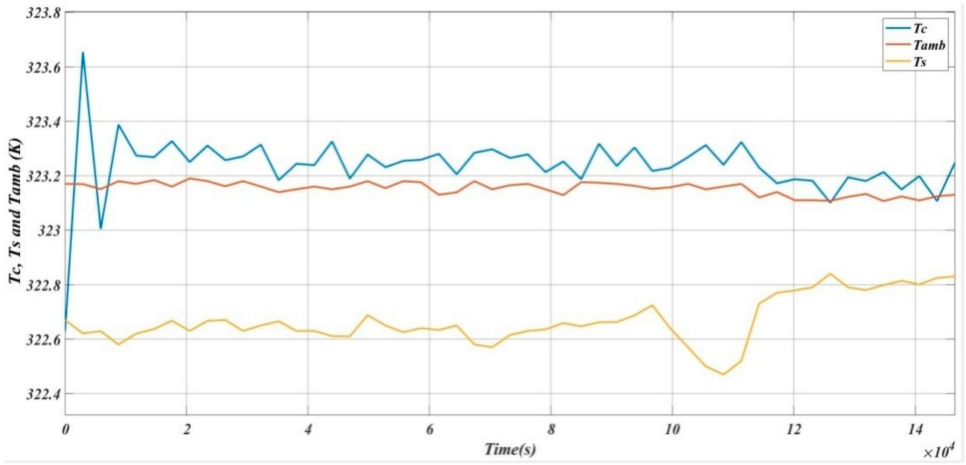

Figure 7. The plot of T_c, T_s and T_{amb} without using KF.

In the subsequent sections, firstly, T_c was estimated using the combined first-order thermal model and KF for three different current profiles and ambient temperatures, which are illustrated in Case 1, Case 2 and Case 3, respectively. Secondly, a similar study was also conducted for the second-order model and finally, the results were compared. All experiments were carried out with different current profiles as per the manufacturer's recommendation to ensure no battery health degradation [58]. In all cases, the initial currents were kept high for rapid charging of the cell.

4.1. Case 1: T_{amb} = 293 K (20 °C)

At first, T_c was initialized to T_s in the simulation as initially, the cell was in a thermal equilibrium state. T_{amb} was considered as 293 K (20 °C), and a very low value of discharging current was applied for the core and surface temperature to rise. The pattern used in Case 1 is shown in Figure 8, and the plot of estimated T_c and measured T_s are shown in Figure 9 whereas the difference between the estimated T_c and measured T_s is shown in Figure 10. It was observed that T_c and T_s closely followed the current pattern, and the maximum difference between estimated T_c and measured T_s was noted as 6.8 K, whilst it was also noticed that for the entire duration, $T_c > T_s$, and the maximum difference occurred when the current was at its peak.

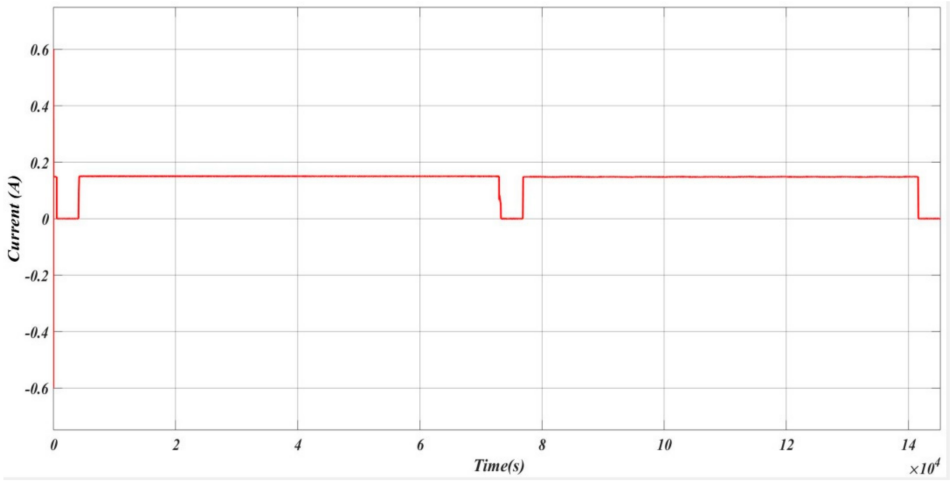

Figure 8. The pattern of the discharging current applied to the cell.

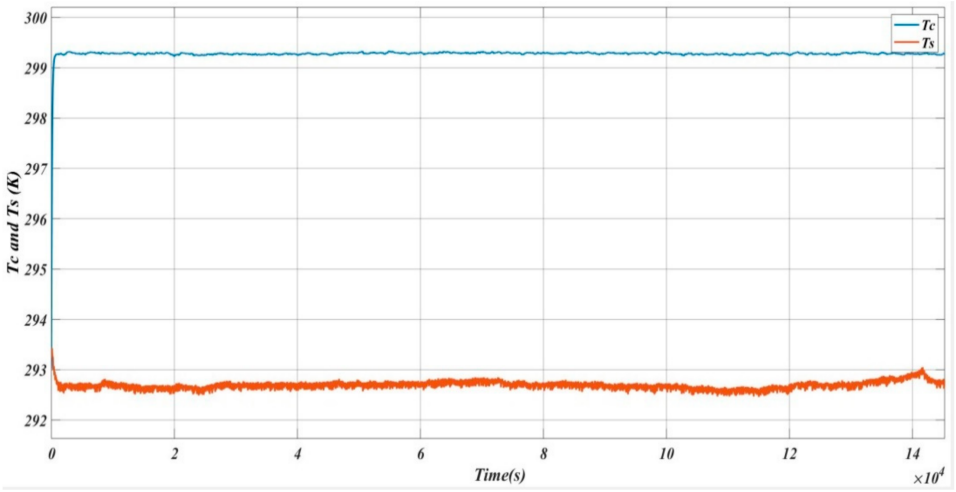

Figure 9. The plot of the estimated T_c and measured T_s.

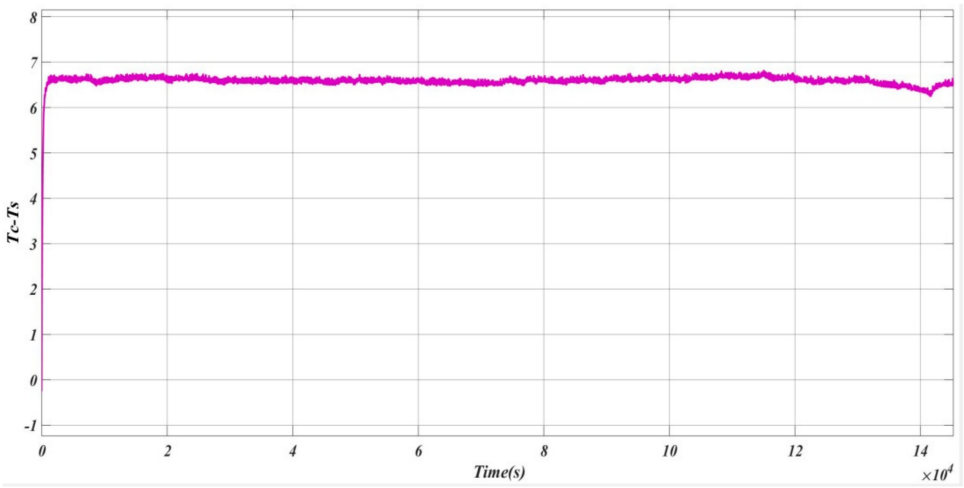

Figure 10. Variation of the difference between the estimated T_c and measured T_s.

4.2. Case 2: T_{amb} = 323 K (50 °C)

In the second phase of the experiments, the temperature of the thermal chamber (T_{amb}) was set to 323 K (50 °C). The pattern used in Case 2 is shown in Figure 11. Similar to Case 1, T_c was initialized to T_s during the simulation here as well. The estimated T_c and measured T_s are shown in Figure 12. It was observed that the temperatures closely followed the current pattern here also. The maximum difference between T_c and measured T_s was noted as 7K. The plot of the difference between the estimated T_c and measured T_s is shown in Figure 13. Similar observations to those made for Case 1 were also noticed here in Case 2 regarding T_c and T_s.

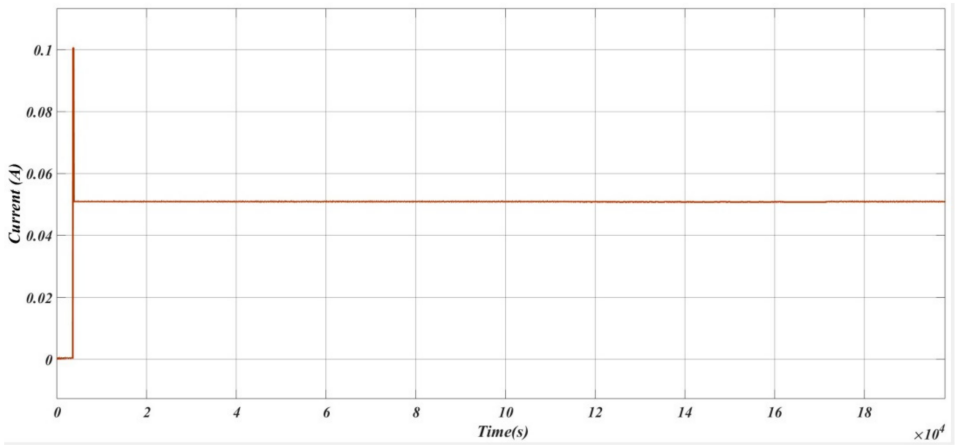

Figure 11. The pattern of the discharging current applied to the cell.

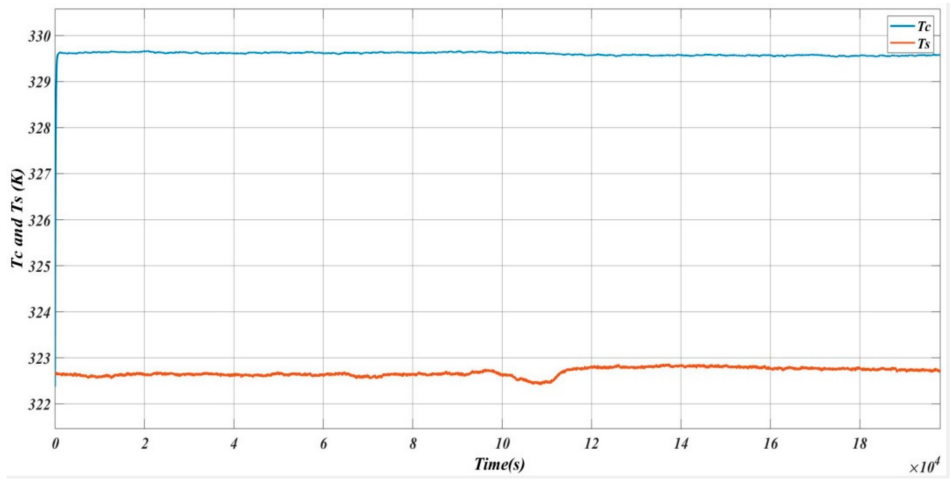

Figure 12. The plot of the estimated T_c and measured T_s.

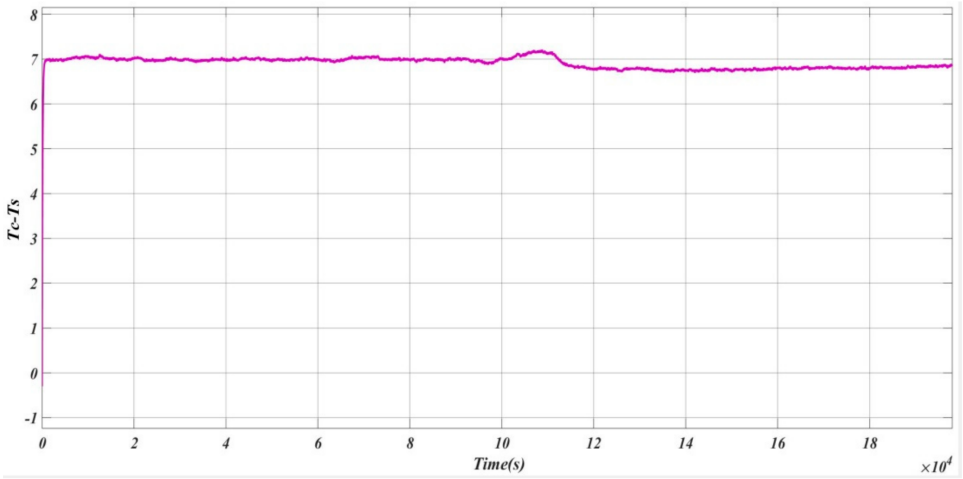

Figure 13. Variation of the difference between the estimated T_c and measured T_s.

4.3. Case 3: T_{amb} =273 K (0 °C)

During Case 3, the temperature of the thermal chamber (T_{amb}) was set to 273 K (0 °C), and T_c was set equal to T_s. The pattern of discharging current applied to the battery is shown in Figure 14. Figure 15 shows the estimated T_c and measured T_s. Figure 16 shows the

difference between the estimated T_c and measured T_s. It can be noticed from Figure 15 that at the beginning the magnitude of T_c and T_s were very large. This was due to the high value of discharging current during this period. It was also observed that the temperature rise is a slow process due to the presence of thermal resistances (R_u and R_c). The temperature difference increased as the value of discharge current increased. Therefore, it can be inferred from these observations that the temperature rise closely follows the current through the battery, and the rate of rising of T_c was the same as T_s for a low value of current. However, for higher values of the current the rise in T_c was much higher than that in T_s. From these observations, the importance of accurate core and surface temperature estimation alongside the requirement of effective and efficient thermal management to maintain T_c under the safe operating limit is evidenced.

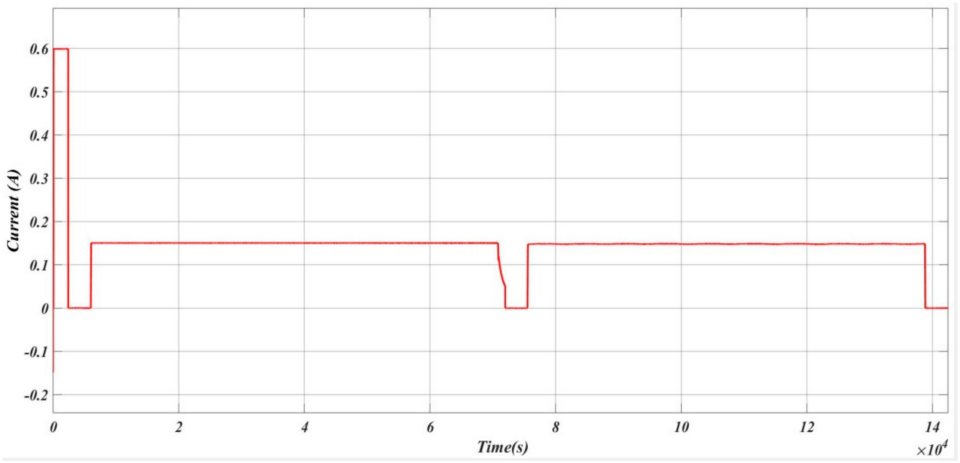

Figure 14. The pattern of the discharging current applied to the cell.

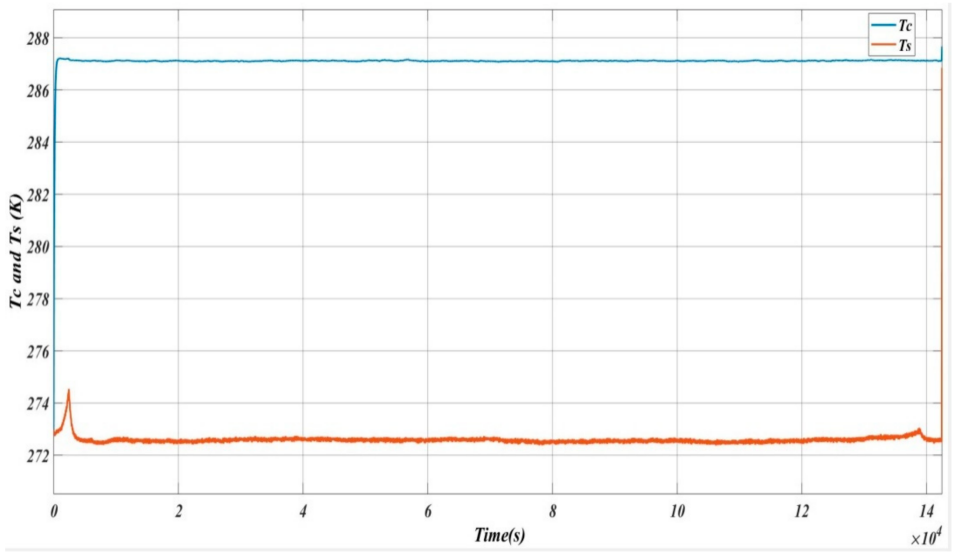

Figure 15. The plot of the estimated T_c and measured T_s.

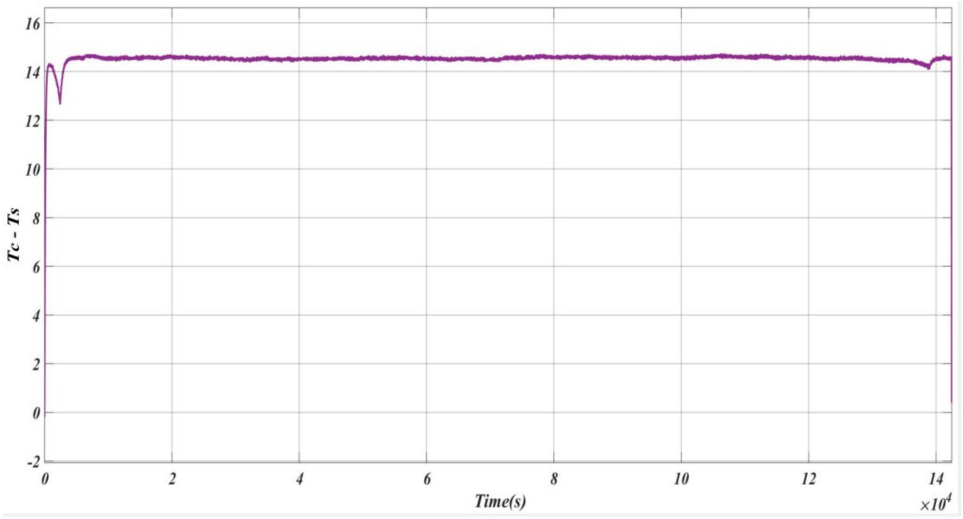

Figure 16. Variation of the difference between the estimated T_c and measured T_s.

4.4. Comparison between First-Order and Second-Order Thermal Models

This section deals with the comparative analysis between the first-order and second-order thermal based on the estimation accuracy, parameter identification, experimental test requirement and suitability for onboard low-cost BMS. To compare the models, the same values of thermal parameters, current, T_s, T_{amb} and Q were injected into the thermal models. Similar current profiles to those used in Case 1, Case 2 and Case 3 of the first-order model were also applied to the second-order thermal model. Heat generation was calculated using the same 1-RC ECM as used in the first-order model. Finally, the estimated T_c profiles obtained from the first-order and second-order thermal models were compared to analyze the prediction accuracy of these models. Figure 17 shows the current profile used for the comparative study, whereas Figures 18 and 19 depict the difference in T_c and T_s obtained from the first-order and second-order thermal model, respectively.

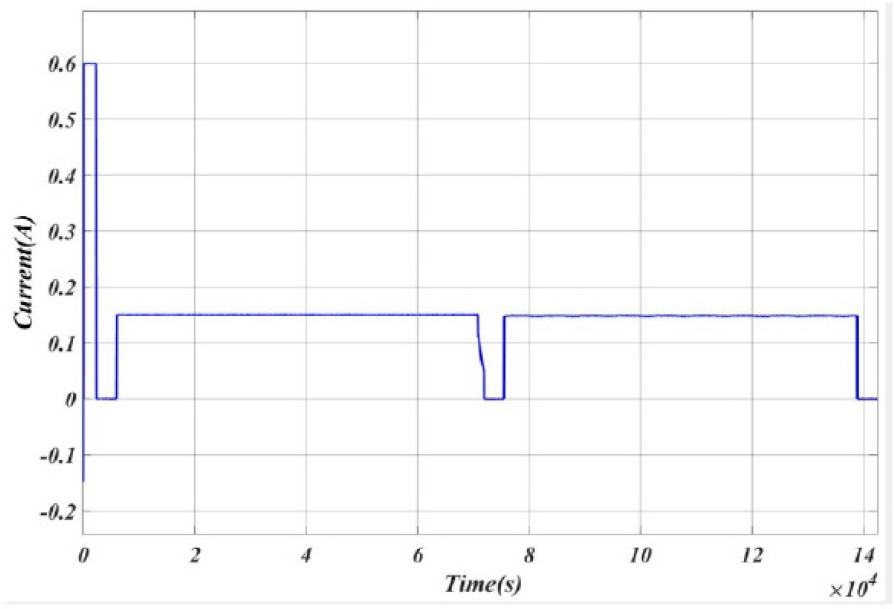

Figure 17. The pattern of the discharging current applied to both the models.

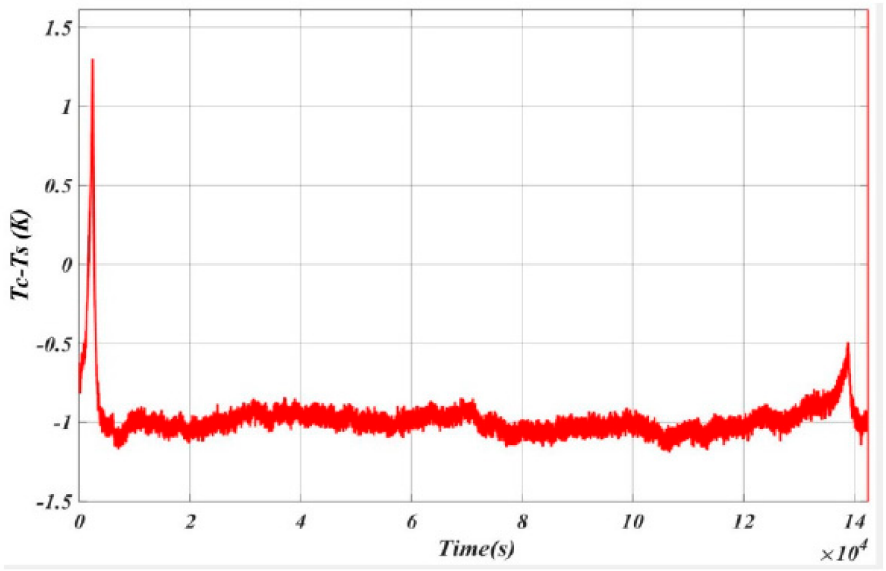

Figure 18. Difference between T_c and T_s obtained from the second-order thermal model.

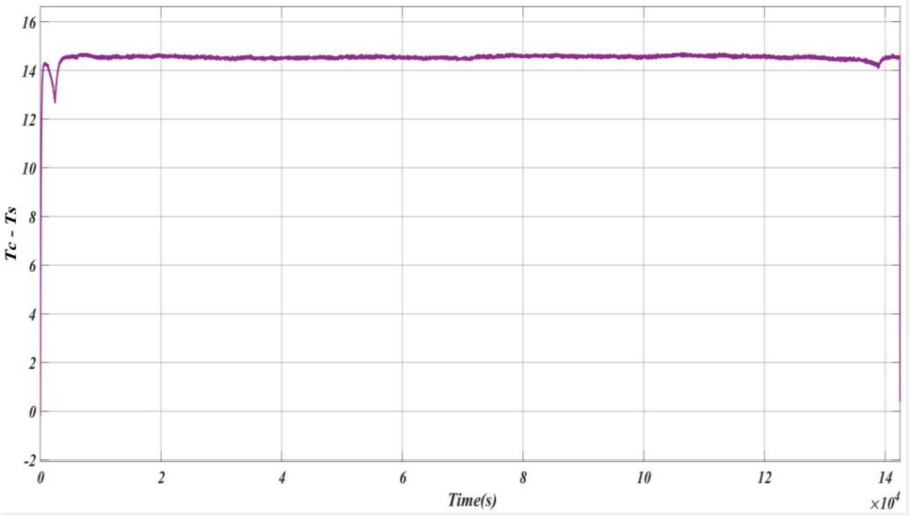

Figure 19. Difference between T_c and T_s obtained from the first-order thermal model.

It was observed that the difference in temperatures was larger in the first-order thermal model due to the change in T_c and not T_s. This is because of the decoupling between T_s and T_c, as seen in Equation (3). Moreover, while comparing Equations (7)–(9) with Equations (12)–(14), it was noticed that the output parameter T_s in KF showed no dependence on the state $T_{c,t-1}$ which is also a major reason behind the estimation error in case of the first-order model. Further, references [43,61] demonstrated that C_c and R_u of the second-order thermal model have a significant effect on T_c. Since these parameters were not present in the C and D matrices of the first-order model, a large increase in T_c was observed. The thermal parameter sensitivity analysis, as conducted in references [8,61], also confirmed the same reason behind the difference in temperature estimation by the first-order thermal model. It was found that the difference between T_s and T_c is increased if the discharge current increases. Hence, for currents with dynamic changes, T_c estimation using the first-order model provides a large difference from the second-order model. Further, C_c only contributed to the transient part of T_c. However, with small changes in R_c and R_u, a large variation in T_c was also observed. The modeling complexity, experimental requirement and computational expenses in the used second-order model were not considerably high compared to the first-order model considered here. A tradeoff between

the modeling complexity and accuracy requirement suggests the implementation of a second-order model is worthwhile for smart BMS, especially for high-power applications of LIB.

4.5. Comparison between First-Order and Second-Order Thermal Models for Higher C Rates

As discussed in the introduction, the performance of different types of battery models is highly influenced by the value of charging–discharging current. As was already witnessed from the above discussion, the second-order model is more accurate compared to the first-order model. However, it is equally important to assess the performance of the second-order model in a high value of discharge current for almost all practical purposes a high value of discharge current is used. Therefore, a discharge current of 5A was applied to both the first and second-order thermal models to observe the change in T_c. and T_s. The difference between the estimated T_c and estimated T_s for the first and second-order thermal models is shown in Figure 20.

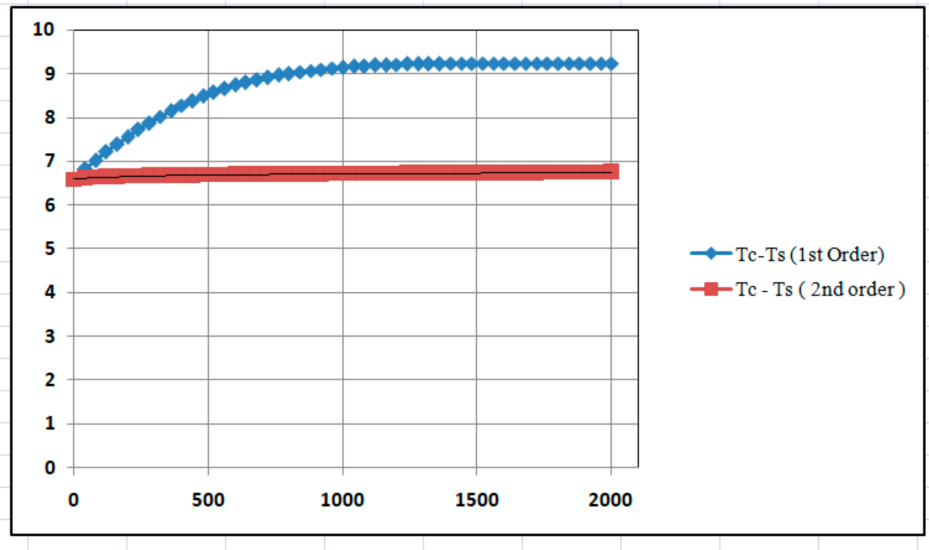

Figure 20. Comparison between T_c-T_s for higher C discharge.

It was observed that the error (T_c-T_s) was higher in the first-order model than in the second-order model. Therefore, it could be concluded that the second-order model can also predict a highly accurate temperature state in practical applications as well.

5. Conclusions

This paper deals with the core temperature (T_c) estimation of lithium-ion 18,650 cell using a Kalman filter (KF). This estimation provides effective thermal management, state estimations, operational safety and the longer useful life of LIB. Initially, a detailed discussion regarding the importance of core and surface temperature estimation was presented followed by a review of the state-of-the-art temperature estimation strategies and thermal modeling of LIB. Equivalent Circuit Models (ECM) of LIB-based heat generation model and heat resistor–capacitor-based thermal models were developed in a MATLAB/Simulink environment. Regarding heat resistor–capacitor-based thermal modeling, one first-order and one second-order thermal model were developed and validated using laboratory experimental data. Further, extensive simulation studies were conducted to demonstrate the influence of battery current and ambient temperature on the core and surface temperature of the LIB cell. The heat transfer equations for a first-order and second-order thermal model were derived, modeled and simulated. KF with appropriate process and measurement noise levels was also used to estimate T_c in terms of measured surface (T_s) and ambient temperature (T_{amb}). Finally, these results were compared to assess the prediction accuracy

of these models. The difference between the core and surface temperatures was noted as approximately 7 K to 8 Kin the first-order model, whereas it was only about 1 K to 2 Kin the second-order thermal model. T_s showed no dependence on T_c in the first-order thermal model. Further, the output parameter T_s in KF showed no dependence on the state $T_{c,t-1}$, which is also a major reason behind the estimation error in the case of the first-order model. The thermal capacitance of core (C_c) and resistances (R_u) of the second-order thermal model have a significant effect on T_c. Since these parameters are not present in the C and D matrices of the first-order model, a large increase in T_c was observed in the first-order thermal model. Hence, the inaccuracy was only due to the error in T_c estimation. The findings are also supported by several other research studies in the domain. Further, the consideration of the thermal capacitance of cell casing and the impact of ambient conditions on the second-order model were the reasons for high accuracy. Further, the performances of first and second-order thermals were also judged with a high value of discharge current for assessing their performance during practical operation. It was observed that the second-order model performance was highly satisfactory compared to the first-order model even in practical applications typically requiring a high value of discharge current. However, estimating the additional parameters of the second-order model requires more experimental data and time. Moreover, due to the complex mathematical form of the second-order model, it takes more computation time. However, looking at the prediction accuracy and the increasing stringent requirement of highly accurate states of battery, it could be stated that it is worth investing more time, cost and expertise in developing a second-order thermal model for more accurate temperature estimation in LIB. This is especially true for the advanced BMS required for high-power LIB packs used in EVs and grid-tied energy storage alongside highly sophisticated consumer electronics. The discussed second-order thermal of a single cell can be extended to an LIB pack by integrating the thermal gradient and the impact of peripheral cells alongside optimal placing of temperature sensors inside the battery casing to adjust the ambient temperature parameter value in the model. All these aspects will be considered in our future research.

Author Contributions: Conceptualization, S.S. and S.W.; methodology, S.S. and A.S.; software, S.S. and A.S.; validation, S.S.; formal analysis, S.S. and A.S.; investigation, S.S. and A.S.; resources, V.M. and S.W.; data curation, V.M.; writing—original draft preparation, S.S. and A.S.; writing—review and editing, A.S. and S.W.; visualization, S.S. and A.S.; supervision, S.W.; All authors have read and agreed to the published version of the manuscript.

Funding: This research received no external funding.

Institutional Review Board Statement: Not applicable.

Informed Consent Statement: Not applicable.

Data Availability Statement: Not applicable.

Conflicts of Interest: The authors declare no conflict of interest. No data/information from Robert Bosch Engineering and Business Solutions Private Limited (RBEI) were used for this work.

References

1. Kleiner, J.; Stuckenberger, M.; Komsiyska, L.; Endisch, C. Advanced Monitoring and Prediction of the Thermal State of Intelligent Battery Cells in Electric Vehicles by Physics-Based and Data-Driven Modeling. *Batteries* **2021**, *7*, 31. [CrossRef]
2. Marcis, V.A.; Kelkar, A.; Williamson, S.S. Electrical circuit modeling of a 18650 lithium-ion cell for charging protocol testing for transportation electrification applications. In Proceedings of the 2020 IEEE Transportation Electrification Conference & Expo (ITEC), Chicago, IL, USA, 23–26 June 2020.
3. Dao, V.Q.; Dinh, M.-C.; Kim, C.S.; Park, M.; Doh, C.-H.; Bae, J.H.; Lee, M.-K.; Liu, J.; Bai, Z. Design of an Effective State of Charge Estimation Method for a Lithium-Ion Battery Pack Using Extended Kalman Filter and Artificial Neural Network. *Energies* **2021**, *14*, 2634. [CrossRef]
4. Marcis, V.A.; Praneeth, A.V.J.S.; Patnaik, L.; Williamson, S.S. Analysis of CT-CV Charging Technique for Lithium-ion and NCM 18650 Cells over Temperature Range. In Proceedings of the Proceedings of the IEEE International Conference on Industrial Technology, Buenos Aires, Argentina, 26–28 February 2020.

5. Li, W.; Zhu, J.; Xia, Y.; Gorji, M.B.; Wierzbicki, T. Data-Driven Safety Envelope of Lithium-Ion Batteries for Electric Vehicles. *Joule* **2019**, *3*, 2703–2715. [CrossRef]
6. Lisbona, D.; Snee, T. A review of hazards associated with primary lithium and lithium-ion batteries. *Process Saf. Environ. Prot.* **2011**, *89*, 434–442. [CrossRef]
7. Kong, L.; Li, C.; Jiang, J.; Pecht, M.G. Li-ion battery fire hazards and safety strategies. *Energies* **2018**, *11*, 2191. [CrossRef]
8. Surya, S.; Marcis, V.; Williamson, S. Core Temperature Estimation for a Lithium ion 18650 Cell. *Energies* **2020**, *14*, 87. [CrossRef]
9. Zhu, J.; Sun, Z.; Wei, X.; Dai, H. Battery internal temperature estimation for LiFePO4 battery based on impedance phase shift under operating conditions. *Energies* **2017**, *10*, 60. [CrossRef]
10. Sidhu, M.S.; Ronanki, D.; Williamson, S. State of charge estimation of lithium-ion batteries using hybrid machine learning technique. In Proceedings of the IECON Proceedings (Industrial Electronics Conference), Lisbon, Portugal, 14–17 October 2019.
11. Sidhu, M.S.; Ronanki, D.; Williamson, S. Hybrid State of Charge Estimation Approach for Lithium-ion Batteries using k-Nearest Neighbour and Gaussian Filter-based Error Cancellation. *IEEE Int. Symp. Ind. Electron.* **2019**, *2019*, 1506–1511. [CrossRef]
12. Samanta, A.; Chowdhuri, S. Active Cell Balancing of Lithium-ion Battery Pack Using Dual DC-DC Converter and Auxiliary Lead-acid Battery. *J. Energy Storage* **2021**, *33*, 102109. [CrossRef]
13. Kelkar, A.; Dasari, Y.; Williamson, S.S. A Comprehensive Review of Power Electronics Enabled Active Battery Cell Balancing for Smart Energy Management. In Proceedings of the 2020 IEEE International Conference on Power Electronics, Smart Grid and Renewable Energy (PESGRE2020), Cochin, India, 2–4 January 2020.
14. Samanta, A.; Chowdhuri, S.; Williamson, S.S. Machine Learning-Based Data-Driven Fault Detection/Diagnosis of Lithium-Ion Battery: A Critical Review. *Electronics* **2021**, *10*, 1309. [CrossRef]
15. Tanim, T.R.; Rahn, C.D.; Wang, C.Y. State of charge estimation of a lithium ion cell based on a temperature dependent and electrolyte enhanced single particle model. *Energy* **2015**, *80*, 731–739. [CrossRef]
16. Farmann, A.; Sauer, D.U. A study on the dependency of the open-circuit voltage on temperature and actual aging state of lithium-ion batteries. *J. Power Sources* **2017**, *347*, 1–13. [CrossRef]
17. Zheng, F.; Jiang, J.; Sun, B.; Zhang, W.; Pecht, M. Temperature dependent power capability estimation of lithium-ion batteries for hybrid electric vehicles. *Energy* **2016**, *113*, 64–75. [CrossRef]
18. Surya, S.; Mn, A. Effect of Fast Discharge of a Battery on its Core Temperature. In Proceedings of the 2020 International Conference on Futuristic Technologies in Control Systems & Renewable Energy (ICFCR), Malappuram, India, 23–24 September 2020. [CrossRef]
19. Li, Z.; Zhang, J.; Wu, B.; Huang, J.; Nie, Z.; Sun, Y.; An, F.; Wu, N. Examining temporal and spatial variations of internal temperature in large-format laminated battery with embedded thermocouples. *J. Power Sources* **2013**, *241*, 536–553. [CrossRef]
20. Robinson, J.B.; Darr, J.A.; Eastwood, D.S.; Hinds, G.; Lee, P.D.; Shearing, P.R.; Taiwo, O.O.; Brett, D.J.L. Non-uniform temperature distribution in Li-ion batteries during discharge-A combined thermal imaging, X-ray micro-tomography and electrochemical impedance approach. *J. Power Sources* **2014**, *252*, 51–57. [CrossRef]
21. Raijmakers, L.H.J.; Danilov, D.L.; Eichel, R.A.; Notten, P.H.L. A review on various temperature-indication methods for Li-ion batteries. *Appl. Energy* **2019**, *240*, 918–945. [CrossRef]
22. Pan, Y.W.; Hua, Y.; Zhou, S.; He, R.; Zhang, Y.; Yang, S.; Liu, X.; Lian, Y.; Yan, X.; Wu, B. A computational multi-node electro-thermal model for large prismatic lithium-ion batteries. *J. Power Sources* **2020**, *459*, 228070. [CrossRef]
23. Sun, F.; Xiong, R.; He, H.; Li, W.; Aussems, J.E.E. Model-based dynamic multi-parameter method for peak power estimation of lithium-ion batteries. *Appl. Energy* **2012**, *96*, 378–386. [CrossRef]
24. Lu, L.; Han, X.; Li, J.; Hua, J.; Ouyang, M. A review on the key issues for lithium-ion battery management in electric vehicles. *J. Power Sources* **2013**, *226*, 272–288. [CrossRef]
25. Ghalkhani, M.; Bahiraei, F.; Nazri, G.A.; Saif, M. Electrochemical–Thermal Model of Pouch-type Lithium-ion Batteries. *Electrochim. Acta* **2017**, *247*, 569–587. [CrossRef]
26. Yang, X.G.; Leng, Y.; Zhang, G.; Ge, S.; Wang, C.Y. Modeling of lithium plating induced aging of lithium-ion batteries: Transition from linear to nonlinear aging. *J. Power Sources* **2017**, *60*, 28–40. [CrossRef]
27. Allafi, W.; Zhang, C.; Uddin, K.; Worwood, D.; Dinh, T.Q.; Ormeno, P.A.; Li, K.; Marco, J. A lumped thermal model of lithium-ion battery cells considering radiative heat transfer. *Appl. Therm. Eng.* **2018**, *143*, 472–481. [CrossRef]
28. Esmaeili, J.; Jannesari, H. Developing heat source term including heat generation at rest condition for Lithium-ion battery pack by up scaling information from cell scale. *Energy Convers. Manag.* **2017**, *139*, 194–205. [CrossRef]
29. Arora, S.; Shen, W.; Kapoor, A. Neural network based computational model for estimation of heat generation in LiFePO4 pouch cells of different nominal capacities. *Comput. Chem. Eng.* **2017**, *101*, 81–94. [CrossRef]
30. Chen, M.; Bai, F.; Song, W.; Lv, J.; Lin, S.; Feng, Z.; Li, Y.; Ding, Y. A multilayer electro-thermal model of pouch battery during normal discharge and internal short circuit process. *Appl. Therm. Eng.* **2017**, *120*, 506–516. [CrossRef]
31. Zhao, Y.; Diaz, L.B.; Patel, Y.; Zhang, T.; Offer, G.J. How to Cool Lithium Ion Batteries: Optimising Cell Design using a Thermally Coupled Model. *J. Electrochem. Soc.* **2019**, *166*, A2849–A2859. [CrossRef]
32. Damay, N.; Forgez, C.; Bichat, M.P.; Friedrich, G. Thermal modeling of large prismatic LiFePO4/graphite battery. Coupled thermal and heat generation models for characterization and simulation. *J. Power Sources* **2015**, *283*, 37–45. [CrossRef]
33. Hu, X.; Liu, W.; Lin, X.; Xie, Y. A Comparative Study of Control-Oriented Thermal Models for Cylindrical Li-Ion Batteries. *IEEE Trans. Transp. Electrif.* **2019**, *5*, 1237–1253. [CrossRef]

34. Xie, Y.; Li, W.; Hu, X.; Zou, C.; Feng, F.; Tang, X. Novel Mesoscale Electrothermal Modeling for Lithium-Ion Batteries. *IEEE Trans. Power Electron.* **2020**, *35*, 2595–2614. [CrossRef]
35. Friesen, A.; Mönnighoff, X.; Börner, M.; Haetge, J.; Schappacher, F.M.; Winter, M. Influence of temperature on the aging behavior of 18650-type lithium ion cells: A comprehensive approach combining electrochemical characterization and post-mortem analysis. *J. Power Sources* **2017**, *342*, 88–97. [CrossRef]
36. Fan, Y.; Bao, Y.; Ling, C.; Chu, Y.; Tan, X.; Yang, S. Experimental study on the thermal management performance of air cooling for high energy density cylindrical lithium-ion batteries. *Appl. Therm. Eng.* **2019**, *155*, 96–109. [CrossRef]
37. Saw, L.H.; Poon, H.M.; Thiam, H.S.; Cai, Z.; Chong, W.T.; Pambudi, N.A.; King, Y.J. Novel thermal management system using mist cooling for lithium-ion battery packs. *Appl. Energy* **2018**, *223*, 146–158. [CrossRef]
38. Liu, B.; Yin, S.; Xu, J. Integrated computation model of lithium-ion battery subject to nail penetration. *Appl. Energy* **2016**, *183*, 278–289. [CrossRef]
39. Doyle, M. Modeling of Galvanostatic Charge and Discharge of the Lithium/Polymer/Insertion Cell. *J. Electrochem. Soc.* **1993**, *140*, 1526–1533. [CrossRef]
40. Xiao, Y.; Fahimi, B. State-space based multi-nodes thermal model for lithium-ion battery. In Proceedings of the 2014 IEEE Transportation Electrification Conference and Expo: Components, Systems, and Power Electronics-From Technology to Business and Public Policy (ITEC 2014), Dearborn, MI, USA, 15–18 June 2014.
41. Tian, N.; Fang, H.; Wang, Y. 3-D Temperature Field Reconstruction for a Lithium-Ion Battery Pack: A Distributed Kalman Filtering Approach. *IEEE Trans. Control Syst. Technol.* **2019**, *27*, 847–854. [CrossRef]
42. Ruan, H.; Jiang, J.; Sun, B.; Gao, W.; Wang, L.; Zhang, W. Online estimation of thermal parameters based on a reduced wide-temperature-range electro-thermal coupled model for lithium-ion batteries. *J. Power Sources* **2018**, *396*, 715–724. [CrossRef]
43. Forgez, C.; Vinh Do, D.; Friedrich, G.; Morcrette, M.; Delacourt, C. Thermal modeling of a cylindrical LiFePO4/graphite lithium-ion battery. *J. Power Sources* **2010**, *195*, 2961–2968. [CrossRef]
44. Dees, D.W.; Battaglia, V.S.; Bélanger, A. Electrochemical modeling of lithium polymer batteries. *J. Power Sources* **2002**, *110*, 310–320. [CrossRef]
45. Lin, X.; Perez, H.E.; Siegel, J.B.; Stefanopoulou, A.G.; Li, Y.; Anderson, R.D.; Ding, Y.; Castanier, M.P. Online parameterization of lumped thermal dynamics in cylindrical lithium ion batteries for core temperature estimation and health monitoring. *IEEE Trans. Control Syst. Technol.* **2013**, *21*, 1745–1755. [CrossRef]
46. Choi, J.W.; Aurbach, D. Promise and reality of post-lithium-ion batteries with high energy densities. *Nat. Rev. Mater.* **2016**, *1*, 16013. [CrossRef]
47. Yang, F.; Wang, D.; Zhao, Y.; Tsui, K.L.; Bae, S.J. A study of the relationship between coulombic efficiency and capacity degradation of commercial lithium-ion batteries. *Energy* **2018**, *145*, 486–495. [CrossRef]
48. Wang, Q.; Zhao, X.; Ye, J.; Sun, Q.; Ping, P.; Sun, J. Thermal response of lithium-ion battery during charging and discharging under adiabatic conditions. *J. Therm. Anal. Calorim.* **2016**, *124*, 417–428. [CrossRef]
49. An, S.J.; Li, J.; Daniel, C.; Kalnaus, S.; Wood, D.L. Design and Demonstration of Three-Electrode Pouch Cells for Lithium-Ion Batteries. *J. Electrochem. Soc.* **2017**, *164*, A1755–A1764. [CrossRef]
50. Patnaik, L.; Williamson, S. A Five-Parameter Analytical Curvefit Model for Open-Circuit Voltage Variation with State-of-Charge of a Rechargeable Battery. In Proceedings of the 2018 IEEE International Conference on Power Electronics, Drives and Energy Systems (PEDES 2018), Chennai, India, 18–21 December 2018.
51. Tran, N.T.; Farrell, T.; Vilathgamuwa, M.; Choi, S.S.; Li, Y. A Computationally Efficient Coupled Electrochemical-Thermal Model for Large Format Cylindrical Lithium Ion Batteries. *J. Electrochem. Soc.* **2019**, *166*, A3059–A3071. [CrossRef]
52. Subramaniam, A.; Kolluri, S.; Santhanagopalan, S.; Subramanian, V.R. An Efficient Electrochemical-Thermal Tanks-in-Series Model for Lithium-Ion Batteries. *J. Electrochem. Soc.* **2020**, *167*, 113506. [CrossRef]
53. Bryden, T.S.; Dimitrov, B.; Hilton, G.; Ponce de León, C.; Bugryniec, P.; Brown, S.; Cumming, D.; Cruden, A. Methodology to determine the heat capacity of lithium-ion cells. *J. Power Sources* **2018**, *395*, 369–378. [CrossRef]
54. Lin, C.; Yu, Q.; Xiong, R.; Wang, L.Y. A study on the impact of open circuit voltage tests on state of charge estimation for lithium-ion batteries. *Appl. Energy* **2017**, *205*, 892–902. [CrossRef]
55. Surya, S.; Channegowda, J.; Datar, S.D.; Jha, A.S.; Victor, A. Accurate battery modeling based on pulse charging using MATLAB/Simulink. In Proceedings of the 9th IEEE International Conference on Power Electronics, Drives and Energy Systems (PEDES 2020), Jaipur, India, 16–19 December 2020.
56. Bernardi, D.; Pawlikowski, E.; Newman, J. A general energy balance for battery systems. *J. Electrochem. Soc.* **1985**, *132*, 5. [CrossRef]
57. Greco, A.; Cao, D.; Jiang, X.; Yang, H. A theoretical and computational study of lithium-ion battery thermal management for electric vehicles using heat pipes. *J. Power Sources* **2014**, *257*, 344–355. [CrossRef]
58. Rao, Z.; Wang, S.; Zhang, G. Simulation and experiment of thermal energy management with phase change material for ageing LiFePO4 power battery. *Energy Convers. Manag.* **2011**, *52*, 3408–3414. [CrossRef]
59. Xie, Y.; Shi, S.; Tang, J.; Wu, H.; Yu, J. Experimental and analytical study on heat generation characteristics of a lithium-ion power battery. *Int. J. Heat Mass Transf.* **2018**, *122*, 884–894. [CrossRef]
60. Chen, L.; Hu, M.; Cao, K.; Li, S.; Su, Z.; Jin, G.; Fu, C. Core temperature estimation based on electro-thermal model of lithium-ion batteries. *Int. J. Energy Res.* **2020**, *44*, 5320–5333. [CrossRef]

61. Surya, S.; Bhesaniya, A.; Gogate, A.; Ankur, R.; Patil, V. Development of thermal model for estimation of core temperature of batteries. *Int. J. Emerg. Electr. Power Syst.* **2020**, *21*, 20200070. [CrossRef]
62. Surya, S.; Patil, V. Cuk Converter as an Efficient Driver for LED. In Proceedings of the 4th International Conference on Electrical, Electronics, Communication, Computer Technologies and Optimization Techniques (ICEECCOT 2019), Mysuru, India, 13–14 December 2019.
63. Lin, X.; Stefanopoulou, A.G.; Perez, H.E.; Siegel, J.B.; Li, Y.; Anderson, R.D. Quadruple adaptive observer of the core temperature in cylindrical Li-ion batteries and their health monitoring. *Proc. Am. Control Conf.* **2012**, *578*, 578–583. [CrossRef]
64. Sun, J.; Wei, G.; Pei, L.; Lu, R.; Song, K.; Wu, C.; Zhu, C. Online internal temperature estimation for lithium-ion batteries based on Kalman filter. *Energies* **2015**, *8*, 4400–4415. [CrossRef]
65. Plett, G. *BatteryManagement Systems, Volume II: Equivalent-Circuit Methods*; Artech: Morristown, NJ, USA, 2015; ISBN 9781630810283.
66. Patnaik, L.; Praneeth, A.V.J.S.; Williamson, S.S. A Closed-Loop Constant-Temperature Constant-Voltage Charging Technique to Reduce Charge Time of Lithium-Ion Batteries. *IEEE Trans. Ind. Electron.* **2019**, *66*, 1059–1067. [CrossRef]
67. Williamson, S.; Vincent, D.; Praneeth, A.; Sang, P.H. Charging Strategies for Electrified Transport. In *Advances in Carbon Management Technologies*; CRC Press: Boca Raton, FL, USA, 2021; pp. 284–302.